THE ASTROPHYSICAL JOURNAL, 430:545–549, 1994 August 1

ULTRAVIOLET IMAGING OF THE AGN + STARBURST GALAXY NGC 1068

SUSAN G. NEFF,[1] MICHAEL N. FANELLI,[1,2] LAURA J. ROBERTS,[3] ROBERT W. O'CONNELL,[4] RALPH BOHLIN,[5]
MORTON S. ROBERTS,[6] ANDREW M. SMITH,[1] AND THEODORE P. STECHER[1]
Received 1993 November 8; accepted 1994 January 20

ABSTRACT

Images of the Seyfert 2 galaxy NGC 1068 were obtained at two ultraviolet wavelengths by the Ultraviolet Imaging Telescope (UIT). These data represent the first detailed UV imagery of a composite (active galactic nucleus + starburst) disk galaxy. NGC 1068 contains multiple components at UV wavelengths: the central active galactic nucleus; a population of very luminous starburst knots; a bright oval inner disk; and a fainter, more circular halo. The most luminous knot, which is located ~750 pc from the nucleus at PA 315°, is ~80 times the luminosity of 30 Doradus and gives NGC 1068 a "double nucleus" appearance in the UV. Significant extended emission is observed throughout the disk, unlike other disk galaxies so far observed in the UV. The radial brightness profile in both UV bandpasses generally follows an exponential decline to ~5 kpc. A faint halo extending to ~13 kpc is likely to be a galaxian-sized reflection nebula where ambient dust scatters the intense UV continuum from the inner galaxy. UV colors show a striking asymmetric morphology, which is correlated with the observed molecular CO emission.

Subject headings: galaxies: active — galaxies: individual (NGC 1068) — galaxies: nuclei — galaxies: Seyfert — ultraviolet: galaxies

1. INTRODUCTION

The well-studied Seyfert 2 galaxy NGC 1068 (M77, 3C 71) is the nearest at $D \sim 15.1$ Mpc and is considered prototypical of "active" galaxies. The near-nuclear region has been well observed over much of the entire electromagnetic spectrum in equisite detail, resulting in the discovery of radio jets originating in the nucleus (Wilson & Willis 1980; Wilson & Ulvestad 1982), broad permitted emission lines in polarized light (Antonucci & Miller 1985), an anisotropic cone of ionizing radiation (Pogge 1988), and resolution of individual clouds in the narrow-line region surrounding the active nucleus (Evans et al. 1991).

Less attention has been focused on the *disk* of NGC 1068, although it has been long noted for morphological peculiarities (e.g., Sandage 1961; Hodge 1968). At $r < 25''$ (1.8 kpc) an unusual high surface brightness disk is observed in optical light and is described by a broken elliptical ring of blue continuum knots and strong nebular line emission. The circumnuclear region emits copious far-IR emission (Telescope & Decher 1988). It is also characterized by a molecular CO ring (Myers & Scoville 1987; Planeas, Scoville, & Myers 1991; Kaneko et al. 1992) and by extended nonthermal radio continuum emission (Wynn-Williams, Becklin, & Scoville 1985). The inner disk is pervaded by a diffuse ionized medium, which is probably powered by scattered nuclear ionizing radiation (Bland-Hawthorn, Sokolowski, & Cecil 1991; Sokolowski, Bland-Hawthorn, & Cecil 1991). Additional optically bright knots are observed to a radius of ~50″ (3.5 kpc) and are embedded within a dusty spiral pattern (e.g., Schild, Tresch-Fienberg, & Huchra 1985; Ichikawa et al. 1987). These knots contain intense massive star formation, as evidenced by their general correspondence with strong Hα emission and by their blue optical colors.

Ultraviolet spectroscopy has been used to explore the active nucleus and the massive star population in a few regions of NGC 1068 using the *IUE* satellite. *IUE* observations (Snijders, Briggs, & Boksenberg 1982) show that NGC 1068 is a multiple source at UV wavelengths. Weedman & Huenemoerder (1985) and Bruhweiler, Truong, & Altner (1991, hereafter BTA91) mapped the circumnuclear region with *IUE* and confirm the presence of many discrete UV sources and of generally low levels of UV extinction. Intense recent star formation is demonstrated by the characteristic spectral morphology of OB stars observed in these spectra. These conclusions are strengthened by *HST*/GHRS observations of one UV source (Hutchings et al. 1991).

In this Paper, we present the first ultraviolet imaging observations of NGC 1068, report on its global UV morphology, and discuss the implications of the observations.

2. OBSERVATIONS AND DATA REDUCTION

NGC 1068 was observed by the Ultraviolet Imaging Telescope (UIT), part of the Astro-1 *Spacelab* observatory, on 1990 December 8. UIT obtained 20 exposures of NGC 1068, using one near-UV (NUV) and three far-UV (FUV) filters during two separate orbital nights. Table 1 provides a summary of the observations. Exposure times were in the ratio 1:5:25:125 to capture the large dynamic range of this system. In this Paper, we discuss only the broad-band imagery obtained through the FUV (B1) and NUV (A1) filters.

UIT images are recorded on IIa-O film with a ~40′ field of view and a spatial resolution of ~2.″5. Flight film was digitized twice with a PDS microdensitometer, first with an image scale of 1.″14 pixel^{-1}, and additionally with an image scale of 0.″56 pixel^{-1}. The smaller scale provides improved sampling of the

[1] Laboratory for Astronomy and Solar Physics, Code 681, NASA/Goddard Space Flight Center, Greenbelt, MD 20771.
[2] National Research Council Postdoctoral Fellow.
[3] Hughes STX Corporation, Code 681, NASA/Goddard Space Flight Center, Greenbelt, MD 20771.
[4] Astronomy Department, University of Virginia, Charlottesville, VA 22903.
[5] Space Telescope Science Institute, 3700 San Martin Drive, Baltimore, MD 21218.
[6] National Radio Astronomy Observatory, Edgemont Road, Charlottesville, VA 22903.

TABLE 1

UIT IMAGERY OF NGC 1068[a]

UIT Image Number	Filter[b]	Exposure Time (s)
FUV344	B1	6.3
FUV345	B1	29.6
FUV346	B1*	752.0
FUV347	B1*	150.0
FUV410	B1*	112.0
FUV411	B1*	563.0
FUV412	B1	22.0
FUV404	B5	113.0
FUV405	B5	563.0
FUV406	B5	22.0
FUV407	B6	10.7
FUV408	B6	55.8
FUV403	B6	1.7
NUV301	A1	6.0
NUV302	A1*	29.6
NUV303	A1*	752.0
NUV304	A1*	149.0
NUV330	A1*	113.0
NUV331	A1*	563.0
NUV332	A1*	22.0

[a] Images used in this Paper are indicated with an asterisk.

[b] The effective wavelength and width of the UV bandpasses are as follows. See Stecher et al. (1992) for a plot of the wavelength dependence of these filters.

B1: $\lambda_{eff} = 1520$ Å, $\Delta\lambda = 354$ Å; B5: $\lambda_{eff} = 1620$ Å, $\Delta\lambda = 225$ Å; B6: $\lambda_{eff} = 1500$ Å, $\Delta\lambda = 400$ Å; A1: $\lambda_{eff} = 2490$ Å, $\Delta\lambda = 1150$ Å.

PSF for well-pointed observations, such as these (Cornett et al. 1994). The spatial resolution is estimated to be $\sim 2''$ for the NUV and $\sim 2''.5$ for the FUV. A more complete discussion of the telescope, detectors, and standard processing of UIT data is in Stecher et al. (1992).

The background in UIT images is a combination of the extraterrestrial UV background, scattered light from the Sun, Moon, and Earth, residual airglow located above the Shuttle's altitude, and the fog level of the film. The average background was subtracted from each image. The estimated background uncertainty is a combination of pixel-to-pixel sensitivity variations and low-amplitude fluctuations produced by uneven fog levels in the film. We determine the sky background to be $\simeq 23.4$ mag arcsec^{-2} in the far-UV, and $\simeq 24.8$ mag arcsec^{-2} in the near-UV. Magnitudes are in the monochromatic system, $m_\lambda = -2.5 \log F_\lambda - 21.1$, where F_λ is the incident flux in ergs s^{-1} cm^{-2} Å^{-1}.

In the case of the NGC 1068 images, the bright nuclear region is saturated in the longer exposures. To explore the full range of UV morphology, saturated regions were masked and the linearly exposed portions of the images were stacked in each filter. Four stacked images were created, using both FUV and NUV images at both image scales. The registration for the NUV stacked imagery is accurate to $\pm 1''$. In the FUV, where few suitable stars are available to guide registration, the morphology of NGC 1068 itself is used, and the alignment is slightly more uncertain. Alignment of the stacked FUV to the NUV image is slightly worse but is adequate to interpret the FUV to NUV color distribution (§ 3.4).

Radial surface brightness profiles are obtained by measuring the integrated flux in circular annuli of increasing radius, on the galaxy nucleus. Photometric errors include uncertainties in the instrumental calibration and background determinations. UV colors are derived, both as a function of radius and in the form of a map within a diameter of 2′.

3. ULTRAVIOLET MORPHOLOGY OF NGC 1068

NGC 1068 exhibits a complex morphology at ultraviolet wavelengths, which is shown in Figures 1 and 2 (Plates 21 and 22). In addition to the strong central source, identified with the active nucleus, a bright oval-inner disk and a population of UV-luminous knots are notable. The global appearance of NGC 1068 is similar to that observed in optical broad-band (*UBV*) images (e.g., Walker 1968; Scoville, Young, & Lucy 1983; Ichikawa et al. 1987) with some important differences. The most striking aspect of Figure 1 is the "double-nucleus" appearance of NGC 1068 in the ultraviolet. The complex of knots $\sim 10''$ northwest of the nucleus, optically unremarkable, contributes significantly to the global UV luminosity and verifies the results of Snijders et al. (1983) and BTA91.

The UV brightness distribution of NGC 1068 is unlike that so far observed in other disk galaxies. In NGC 1068, the knots are embedded in a strong extended UV background which prevades both the arm and interarm regions and which extends to greater radii than the knot population. Most disk galaxies are better characterized by a "beads-on-a-string" morphology, where high surface brightness discrete sources trace spiral arms (e.g., M81, Hill et al. 1992) and any diffuse emission tends to occur along the spiral arms (e.g., M101, Stecher et al. 1982; M74, Cornett et al. 1994; M33, Buta et al. 1993).

External to the bright inner disk, lower surface brightness emission is observed, appearing more circular at increasing radius. This outer region extends to a radius of $\sim 1'$ (4 kpc) in the FUV, and $\sim 3'$ (13 kpc) in the NUV. The latter value is $\sim 85\%$ of the isophotal radius of 3′.45 at $\mu_B = 25$ mag arcsec^{-2} (de Vaucouleurs, de Vaucouleurs, & Corwin 1976). In the NUV the relative integrated fluxes of the active nucleus, the inner disk, and the outer disk are found to be 1:3.8:1. *Therefore the active nucleus does not dominate the global UV luminosity.* Each of these structures are discussed individually in the following subsections.

3.1. *The Nuclear Region* ($r < 5''$)

The strong central continuum peak associated with the active galactic nucleus (AGN) is not resolved by UIT. The FUV flux is $\sim 6 \times 10^{-14}$ ergs cm^{-2} s^{-1} Å^{-1} within $8''$; the (FUV − NUV) color within the same radius is $\simeq -0.33$, consistent with the values derived by convolving the UIT filters with the *IUE* spectrum of Kinney et al. (1993).

Inspection of the images indicates the circumnuclear emission is not axisymmetric. The UV light is extended toward the northeast, at PA $\sim 35°$, in agreement with the radio jet axis (Wilson & Ulvestad 1982). Pogge & DeRobertis (1993) find a similar result from ground-based optical imagery at 3600 Å. The asymmetry is observed in both UV bandpasses, and probably results from scattered nuclear continuum radiation.

3.2. *The "Starburst" Knots*

The UIT images show the extent and luminosity of the "starburst" knots described by BTA91 as well as several others. The UV colors of the more prominent knots are given in Table 2; each region is identified by letter in Figure 3. Colors in Table 2 refer to the entire region indicated, some of which

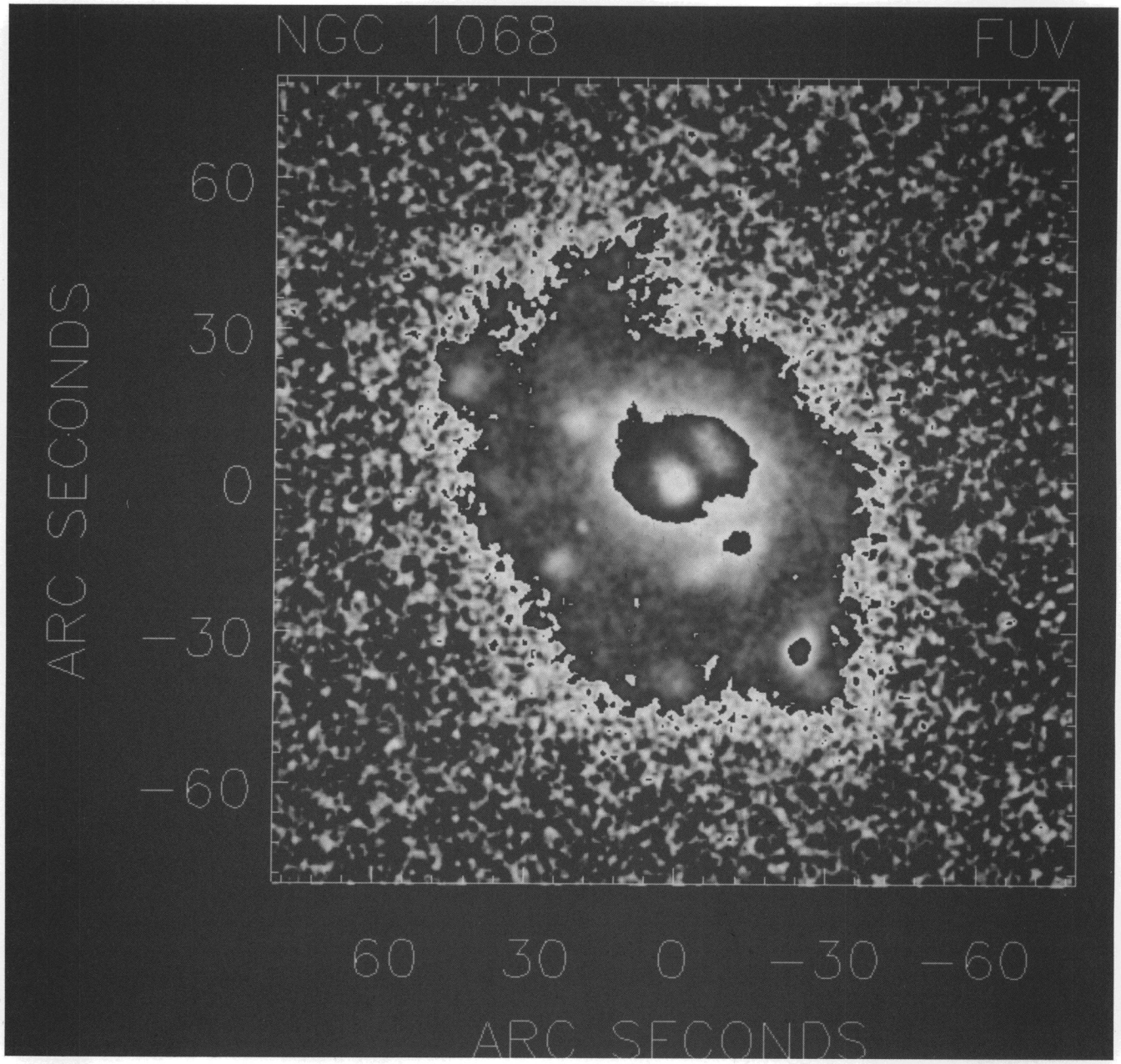

FIG. 1.—UIT far-UV (FUV ≡ 1520 Å) image of NGC 1068, centered at R.A. = $2^h40^m07^s.2$, Decl. = −00°13′30″. This image is the sum of four UIT frames totaling 1577 s. For D = 15.1 Mpc, 1″ ≃ 70 pc. The color table has been wrapped three times. Peak surface brightness at the nucleus is ∼16.2 mag arcsec^{-2}. In addition to the bright, unresolved AGN and the population of luminous knots, NGC 1068 exhibits discernible emission *throughout* the disk. The circumnuclear emission is asymmetric and extended toward PA 35°. The most striking aspect of the UV morphology is the prominence of the knots, especially the region 10″ northwest of the AGN, which appears to be a "second" nucleus.

NEFF et al. (see 430, 546)

PLATE 22

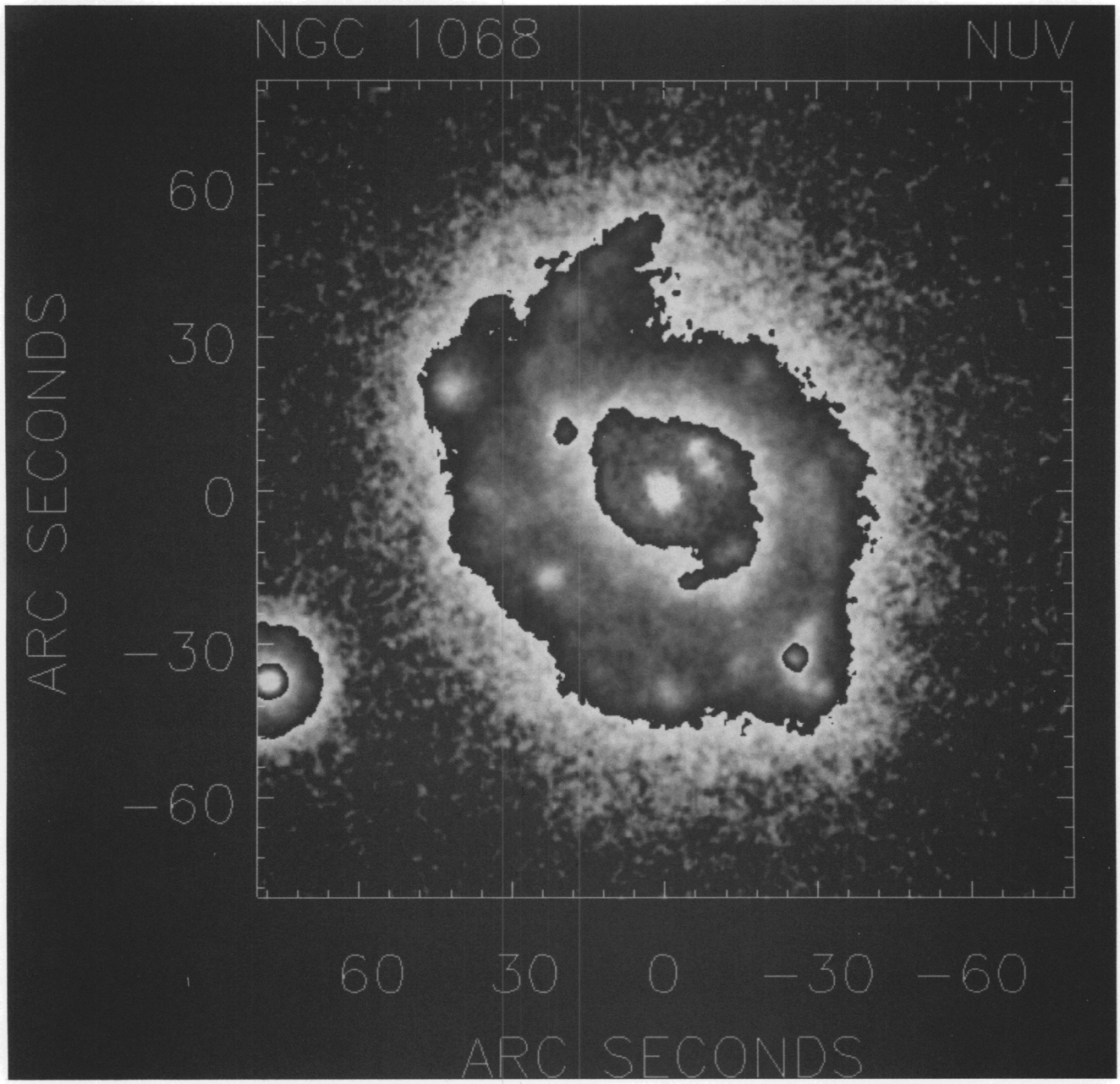

FIG. 2.—UIT near-UV (NUV ≡ 2490 Å) image at the same angular and intensity scale as Fig. 1. This image is the sum of five UIT frames totaling 1606 s. Peak surface brightness at the nucleus is ~ 16.9 mag arcsec^{-2}.

NEFF et al. (see 430, 546)

TABLE 2

PROPERTIES OF UV CONTINUUM KNOTS IN NGC 1068

Identifications (1)	(2)	Position (3)	Size (4)	FUV − NUV (mag) (5)	Luminosity × 30 Dor (6)
A	...	+42″, +19″	8″	−0.23 ± 0.08	4.4
B	...	+36 , −01	8	−0.19 ± 0.12	2.8
C	...	+23 , −16	8	−0.34 ± 0.07	4.8
D	...	−01 , −40	8	−0.27 ± 0.10	3.3
E	...	−25 , −33	8	−0.13 ± 0.03	12
F	...	−29 , −35	14″ × 19″	−0.09 ± 0.03	27
G	9	+19 , +12	8	+0.00 ± 0.03	8.0
H	...	−06 , −17	6 × 7	+0.10 ± 0.05	6.4
I	8a, b	−14 , −11	9 × 10	+0.25 ± 0.03	22
J	1, 2, 3	−08 , +07	7 × 11	−0.36 ± 0.03	78
Nucleus	...	+00 , +00	4.5	−0.77 ± 0.03	

Col. (1): Labels used in this paper; Col. (2): Corresponding identifications from BTA91; Col. (3): Position in arcseconds (+E–W, +N–S) relative to the nucleus; Col. (4): Aperture size in arcseconds. Single values refer to aperture diameter; Col. (5): UV colors derived from the B1 and A1 filters; Col. (6): Relative luminosity of each region scaled to that of 30 Doradus at 1550 Å. The integrated flux of 30 Dor at 1550 Å = 2.82×10^{-11} ergs cm^{-2} s^{-1} Å^{-1} (Israel & Koornneef 1979).

contain several clumps only marginally resolved by UIT. Typical values at the flux maxima are (FUV − NUV) ∼ −1.1 mag. For comparison, the UV color for unreddened early-O stars is ≃ −1.32 mag, for early-B stars ≃ −1.15 mag (Fanelli 1993), while the color of a 5 Myr star cluster is ∼ −1.2 mag in the absence of extinction. The blue UV colors toward many of the knots implies little extinction and large numbers of recently formed massive stars.

The knot complex ∼10″ northwest of the nucleus at PA 315° (region J) is exceptionally bright; its FUV flux ≃30% of the nuclear flux. Our data show additional bright knots, at larger radii than mapped by BTA91, such as the wedge-shaped knot ∼42″ southwest (region E/F) of the nucleus and the string of regions tracing an outer spiral arm (A–D). The observed UV colors of the knots, coupled with the spectral morphology observed by BTA91, demonstrate that the UV light is produced by recently formed massive OB stars. The strength of this star formation can be characterized by comparing these knots with 30 Doradus, the prototypical giant extragalactic H II region in the LMC. In Table 2, we give the relative FUV luminosity of each region with respect to 30 Doradus (uncorrected for extinction). The total UV luminosity of region J is ∼80 times that of 30 Doradus, and even the faintest knots listed in Table 2 are comparable to 30 Dor.

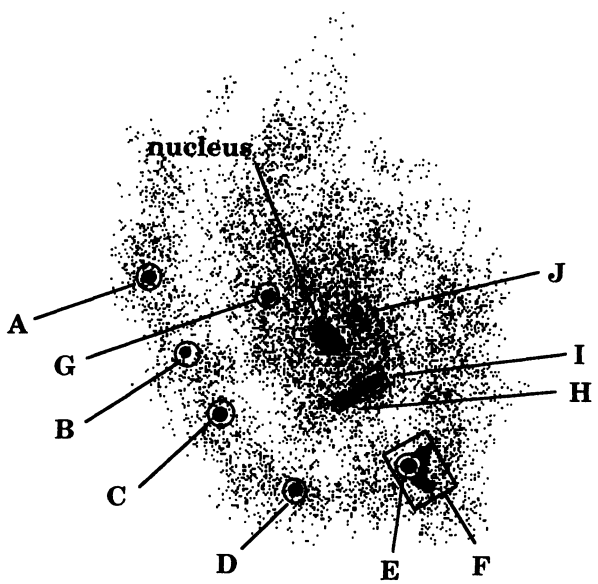

FIG. 3.—Schematic of the UV morphology of NGC 1068 to identify important features. The most prominent knots are labeled A–J, their (FUV − NUV) colors are given in Table 2.

3.3. *The Disk* (5″ < *r* < 60″)

UIT images show an unusual bright inner disk surrounding the nucleus and extending to ∼25″ (1.8 kpc). This disk is atypical of spiral galaxies observed in the UV. In NGC 1068 significant diffuse emission is found at all position angles. A comparison can be made to the structure of M81 (Hill et al. 1992, see Figs. 1 and 2), where bright knots define the spiral pattern, negligible emission is observed in the interarm regions, and only modest emission between knots within the spiral arms. This effect is much more pronouced in the FUV bandpass.

Both FUV and NUV radial surface brightness profiles are derived using concentric circular apertures, centered on the nucleus; the profiles are shown in Figure 4. An exponential profile is displayed for comparison. Excluding the nuclear region, the FUV data follow an exponential profile to the detection limit. Peaks near ∼12″ and ∼43″ are due to the confluence of bright knots (regions J and E/F, respectively) at these radii, and these features are also observed in the optical (e.g., Schild et al. 1985). The NUV generally follows an exponential decline to ∼80″ (5.6 kpc). However, in the NUV a much shallower gradient is observed at larger radii than in the galaxy's central region. We label this extended emission the "halo," and discuss it further in § 3.5.

Several sources probably contribute to the integrated ultraviolet emission of NGC 1068: dust and electron scattered radiation from the AGN, direct light from the OB stars in the knots, reflected light from dust clouds subject to the intense UV radiation of the AGN and knots, and line and continuous emission from the ionized medium. The global disk UV emission is probably dominated by the massive star formation in the knots, with much of the diffuse disk emission produced by UV continuum escaping the knots and, subsequently, scattered by dust.

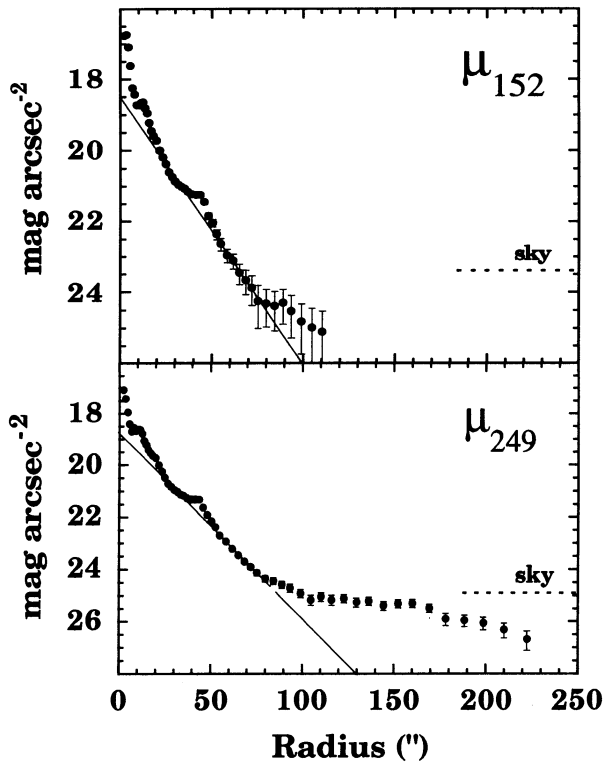

FIG. 4.—Radial surface brightness profiles in the FUV (152 nm) and NUV (249 nm) bandpasses for NGC 1068. Mean surface brightness in magnitudes per arcsec^{-2} within concentric circular annuloi is plotted vs. radius in arcseconds. Exponential profiles are drawn for comparison but are not fits to the data. The disk is detectable in the NUV over 6 mag. The UV light follows an exponential profile in both bandpasses with enhancements at the locations of the most luminous knots; the outer halo lies above an exponential profile.

3.4. *The UV Color Morphology of the Disk*

A radial color profile, derived from the circular aperture photometry discussed above, is shown in Figure 5. The active nucleus is very blue as expected; we find a blue "dip" near a radius of 12″ produced by region J, and a red "peak" near 19″. For $25'' < r < 50''$ (FUV − NUV) $\simeq -0.1$. At larger radii, a slightly red gradient is observed, with (FUV − NUV) reaching ~ 0.08 mag at $r = 75''$ (5.2 kpc); this UV color corresponds to an early-A spectral type and is substantially redder than the cores of the starburst knots.

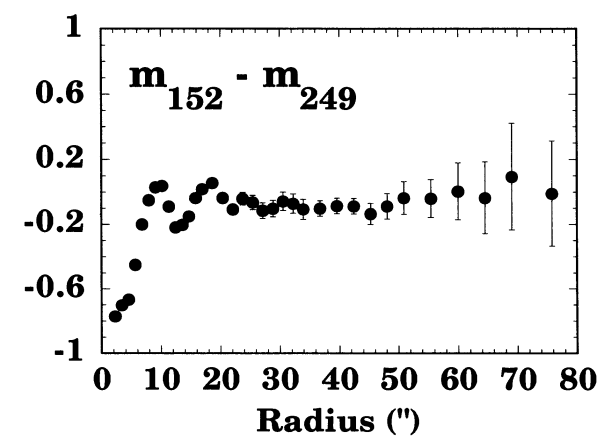

FIG. 5.—Radial UV color profile for NGC 1068, derived from the concentric annular photometry shown in Fig. 4. Blue "dips" correspond to annuli with prominent star-forming knots, whereas red "peaks" correspond to areas of higher extinction and are correlated with the location of molecular gas and dust.

The UV color and morphology of the disk can be further explored through examination of a UV color map [$\equiv -2.5 \times \log F_{FUV}/F_{NUV}$ (Fig. 6 [Pl. 23]). Distinct structures are observed in the UV color map. Both the nucleus and region J are blue (FUV − NUV) ≈ -1.1 to -0.7, as is the disk north and northwest of the nucleus. A striking arc-shaped region of redder color, (FUV − NUV) $\approx +0.35$ to $+0.45$, extends through $\sim 180°$ at a distance of $\sim 20''$ (1.4 kpc) from the nucleus. This arc, which produces the local maximum in the radial color profile mentioned above, is coincident with the southern arc of the molecular ring observed by Planeas et al. (1991), and Kaneko et al. (1992). The soutwest end of the arc terminates in a region containing several "blobs" of redder color, which are coincident with knots H/I.

The disk morphology at UV wavelengths is similar to that observed in the optical ($B-V$) and ($B-I$) color maps presented by Ichikawa et al. (1987). The striking difference in appearance between the strong H II regions J and I is likely to arise from their relative locations with respect to the main volume of molecular gas and dust. We suggest that most of the molecular gas in the direction of J is behind the knot, whereas region I is still largely shrouded in dust. Some UV light escapes from region I, but most is absorbed locally, producing IR dust emission (Telescope & Decher 1988).

3.5. *The Halo* ($1' < r < 3'$)

External to the bright disk described in § 3.3, faint extended emission is observed at $\mu_{NUV} \sim 25.3$ mag arcsec^{-2} ($\sim 60\%$ of the NUV sky level) and extends $\sim 3'$ from the nucleus. This "halo," shown in Figure 7 (Plate 24), is present at all position angles and its brighter segments are spatially correlated with the outer disk or ring observed in the optical (e.g., Hodge 1968). It is not detected in the FUV where the data are noisier. The limit of our NUV photometry, $\mu_{249} > 26$, even on these relatively short exposures, illustrates the darkness of the NUV sky.

The extended emission may be merely the NUV flux from the stellar component responsible for the optical light. No detailed differential optical photometry exists for NGC 1068 at these radii; but extrapolation of the light profiles of Schild et al. (1985) and Ichikawa et al. (1987), along with the results of Hodge (1968) predict $\mu_V \sim 24$–25 at radii of 2–3′. The predicted (NUV − V) color is ~ 0–1 mag, which is too blue for the expected color of an old disk population, but which is consistent with very low levels of continuous star formation.

The central region of NGC 1068 is an intense NUV source. Therefore, the UV "halo" may be a galaxian-sized reflection nebula. We used the method of Stecher et al. (1982) and Jura (1980) to model the surface brightness in the UV halo as scattered light originating in the central regions of the galaxy. With $F_{NUV} = 2.22 \times 10^{-13}$ ergs cm^{-2} s^{-1} Å^{-1} for $r < 60''$, we predict the NUV surface brightness at a radius of 150″ due to isotropically scattered light to be ≈ 24.2 mag arcsec^{-2} for $(\tau a) \simeq 1$, and ≈ 25.5 mag arcsec^{-2} for $(\tau a) \simeq 0.3$, where τ is the optical depth of the dust to the source, and a is the albedo. The observed surface brightness at large radii is consistent with light scattered from the intense UV flux of the inner galaxy.

4. IMPLICATIONS

In § 3 we describe the global morphology of NGC 1068 in the near- and far-UV wavelength ranges. Future papers will discuss the UV/optical light distribution, dust content,

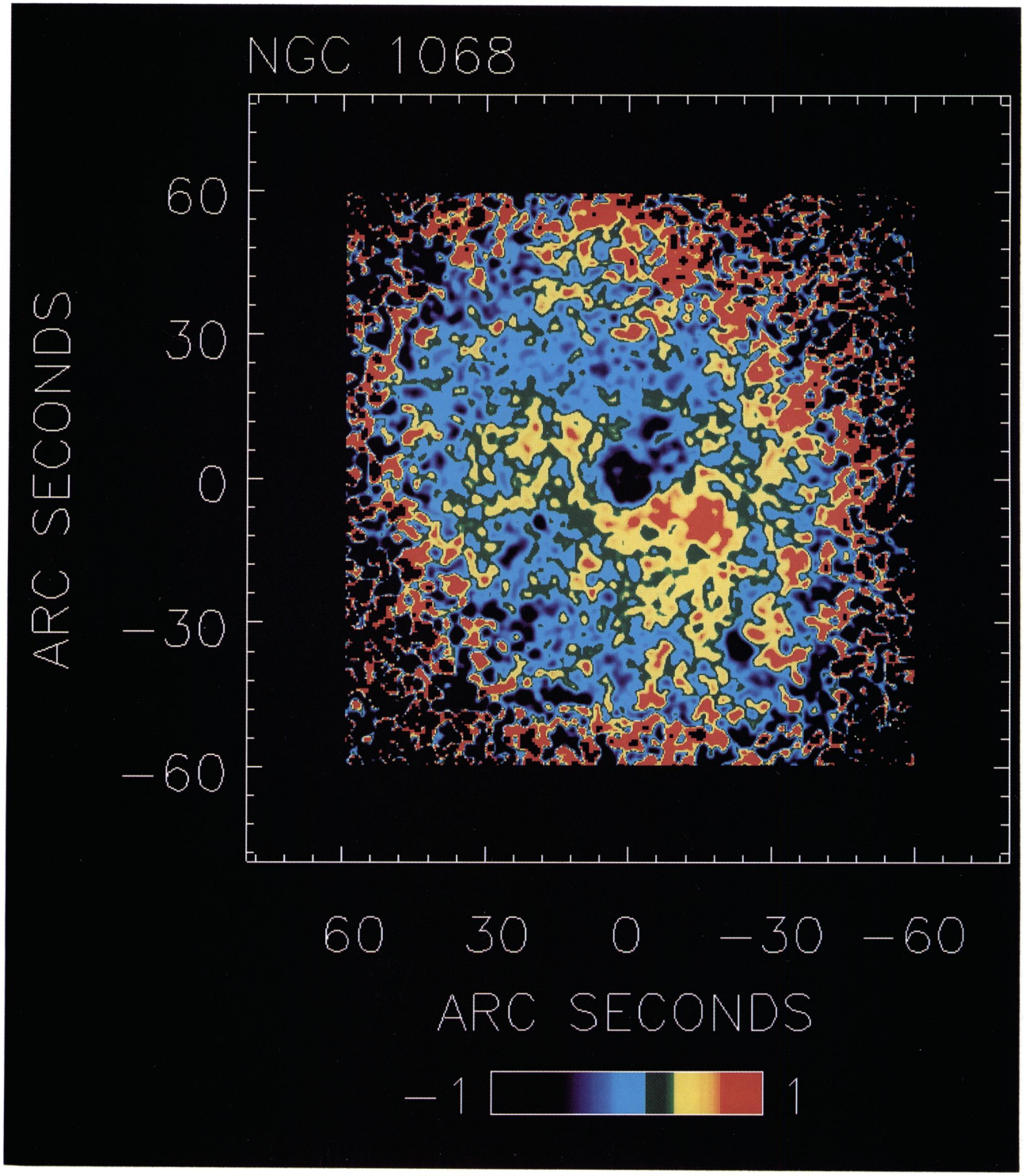

FIG. 6.—A color map [$-2.5 \times \log (F_{FUV}/F_{NUV})$] of the inner disk of NGC 1068. Colors are displayed within a range of -1 to $+1$ mags; the corresponding color for unreddened early-O stars is ~ -1.3 mag. The image shows over a magnitude variation in UV color indicating strongly nonuniform extinction. The color distribution is distinctly asymmetric: north and northeast of the nucleus is a blue [(FUV − NUV) < 0] region; southeast of the nucleus an arc of redder color extends $\sim 180°$. This arc is coincident with the southern molecular arm (Planeas et al. 1991). Extinction from dust is the dominant process producing the observed color distribution. The very blue UV color of the knot 10″ northwest of the nucleus implies a virtually clear line of sight.

NEFF et al. (see 430, 548)

PLATE 24

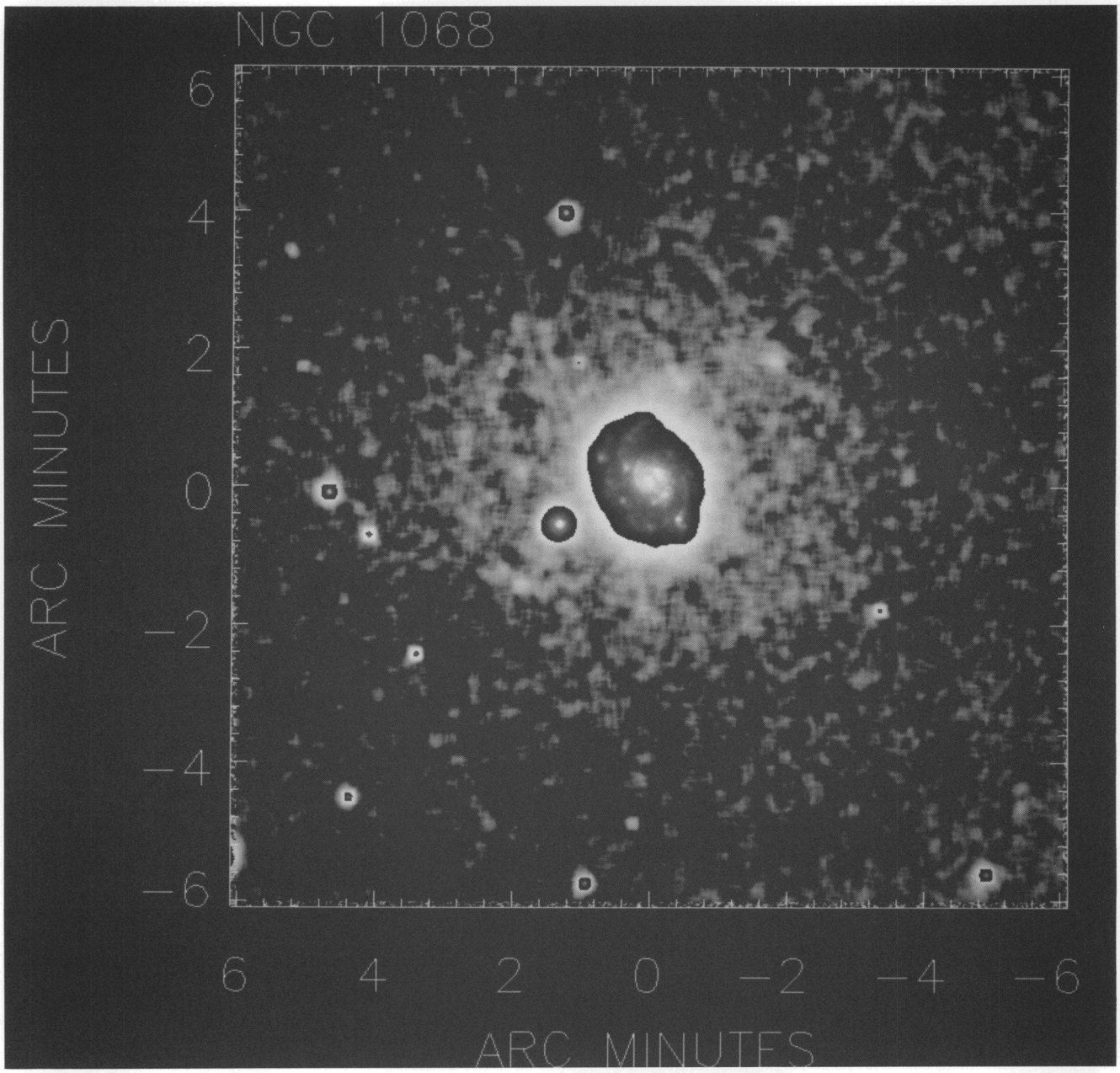

FIG. 7.—UIT near-UV image of NGC 1068. Lower surface brightness features have been smoothed to a resolution of 10″. External to the bright inner disk, a faint extended UV halo is present, with $\mu_{249} \approx 25.3$ mag arcsec^{-2} beyond a radius of $\sim 100''$ (7 kpc). This halo is roughly circular in appearance, unlike the inner disk, and its brighter regions are spatially coincident with the outer disk that is seen in deep optical images. The integrated NUV flux of the halo is comparable to that of the AGN, and its observed surface brightness is consistent with that expected from a simple model of dust scattering the intense UV continuum from the inner galaxy.

NEFF et al. (see 430, 548)

stellar populations, and massive star formation in greater detail. Here we briefly comment on some implications of these observations.

NGC 1068 has an AGN and regions of intense massive star formation existing in close proximity. Separating these components requires high spatial resolution and a multiwavelength approach, made possible here by the low redshift of this system. At larger redshift, the signatures of both types of activity would merge and hinder easy interpretation of more distant active galaxies. Preliminary evidence indicates that even NGC 1068 harbors distinct near-nuclear structures at a scale of a few arcsecs (e.g., Lynds et al. 1991), unresolved by UIT.

Our UV data emphasizes the potential importance of scattered light in UV-bright, dusty systems. Some radio sources at high redshift are found to have aligned optical and radio structures (McCarthy et al. 1987; Chambers, Miley, & van Bruegel 1987), which are variously interpreted as jet-induced star formation (Eales & Rawlings 1990), scattered nuclear radiation (Scarrott, Rolph, & Tadhunter 1990), or both (Miley et al. 1992). These systems are observed in their rest-frame UV bandpass and are more luminous than NGC 1068. The detection of dust-scattered UV continuum in the halo and possibly in the disk of NGC 1068 implies that any dust associated with the gas in the distant aligned systems may contribute to the observed flux. From the Lyα/Hα ratio, McCarthy et al. (1992) have reported modest extinction from dust in two objects at $z > 2$. The aligned structures in distant radio galaxies may be enormous reflection nebulae.

The UV luminosity of NGC 1068 is somewhat surprising, since there are large amounts of distributed dust (Telesco et al. 1984; Telesco & Decher 1988). The "starburst" knots in NGC 1068 are clearly detected and are not strongly extincted. Dusty starburst systems can be bright both the UV and the thermal infrared, a result also found in NGC 6240 (Smith et al. 1992), an IR-luminous and very dusty system. The UV colors observed in some regions of NGC 1068 indicate a line of sight that is nearly clear. We strongly encourage further UV studies of starburst systems, even those that are strong IR thermal sources.

Finally, we note that UV images are a powerful discriminant for spatially mapping extinction in active star-forming systems. While extinction may certainly be studied with good-quality optical data, UV imagery provides a larger amplitude for color variations, due to the wider range of intrinsic stellar colors and the increased amplitude of dust opacity. For comparable photometric precision, UV + optical imagery provides superior accuracy in determining extinction properties, as well as stellar population characteristics.

Hundreds of people contributed to the success of the Astro-1 mission and the UIT experiment; we gratefully acknowledge them collectively here. Funding for the UIT project has been through the Spacelab Office of NASA Headquarters under the project number 440-51. Parts of this research were also supported by NASA grants NAG5-700 and NAGW-2596 to the University of Virginia.

REFERENCES

Antonucci, R. R., & Miller, J. S. 1985, ApJ, 297, 621
Bland-Hawthorn, J., Sokolowski, J., & Cecil, G. 1991, ApJ, 375, 78
Bruhweiler, F. C., Truong, K. Q., & Altner, B. 1991, ApJ, 379, 596 (BTA91)
Buat, V., Vuillemin, A., Burgarella, D., Milliard, B., & Donas, J. 1993, A&A, in press
Chambers, K. C., Miley, G. K., & van Breugel, W. 1987, Nature, 329, 604
Cornett, R. H., et al. 1994, ApJ, submitted
de Vaucouleurs, G., de Vaucouleurs, A., & Corwin, H. G. 1976, Second Reference Catalogue of Bright Galaxies (Austin: Univ. Texas Press)
Eales, S. A., & Rawlings, S. 1990, MNRAS, 243, 1P
Evans, I. N., Ford, H. C., Kinney, A. L., Antonucci, R. R., Armus, L., & Caganoff, S. 1991, ApJ, 269, L27
Fanelli, M. N. 1993, in preparation
Hill, J. K., et al. 1992, ApJ, 395, L37
Hodge, P. W. 1968, AJ, 846
Hutchings, J. B., et al. 1991, ApJ, 377, L25
Ichikawa, S., Okamura, S., Kaneko, N., Nishimura, M., & Toyama, K. 1987, PASJ, 39, 411
Israel, F. P., & Koornneef, J. 1979, ApJ, 390, 403
Jura, M. 1980, ApJ, 241, 965
Kaneko, N., Morita, K., Fukui, Y., Takhashi, N., Sugitani, K., Nakai, N., & Morita, K.-I. 1992, PASJ, 44, 341
Kinney, A. L., Bohlin, R. C., Calzetti, D., Panagia, N., & Wyse, R. F. G. 1993, ApJS, 86, 5
Lynds, R., et al. 1991, ApJ, 369, L31
McCarthy, P. J., Elston, R., & Eisenhardt, P. 1992, ApJ, 387, L29
McCarthy, P. J., van Breugel, W., Spinard, H., & Djorgovski, S. 1987, ApJ, 321, L29
Miley, G., Roettgering, K., Chambers, K., Hunstead, R., Macchetto, F., Roland, J., Schilizzi, R., & van Ojik, R. 1992, ESO Messenger, 68, 12
Myers, S. T., & Scoville, N. Z. 1987, ApJ, 312, L39
Planeas, P., Scoville, N., & Myers, S. T. 1991, ApJ, 369, 364
Pogge, R. W. 1988, ApJ, 328, 519
Pogge, R. W., & DeRobertis, M. M. 1993, ApJ, 404, 563
Sandage, A. R. 1961, The Hubble Atlas of Galaxies (Washington, DC: Carnegie Institute of Washington)
Scarott, S. M., Rolph, C. D., & Tadhunter, C. N. 1990, MNRAS, 243, 5P
Schild, R., Tresch-Fienberg, R., & Huchra, J. 1985, AJ, 90, 441
Scoville, N. Z., Young, J. S., & Lucy, L. B. 1983, ApJ, 270, 443
Smith, A. S., Hill, R. S., Vrba, F. J., & Timothy, J. G. 1992, ApJ, 391, L81
Snijders, M. A. J., Briggs, S. A., & Boksenberg, A. 1982, in Proc. of 3d European *IUE* Conference, ed. M. Grewing (ESA SP-176), 551
Sokolowski, J., Bland-Hawthorn, J., & Cecil, G. 1991, ApJ, 375, 583
Stecher, T. P., Bohlin, R. C., Hill, J. K., & Jura, M. A. 1982, ApJ, 255, L99
Stecher, T. P., et al. 1992, ApJ, 395, L1
Telesco, C. M., Becklin, E. E., Wynn-Williams, C. G., & Harper, D. A. 1984, ApJ, 282, 427
Telesco, C. M., & Decher, R. 1988, ApJ, 334, 573
Walker, M. F. 1968, ApJ, 151, 71
Weedman, D. W., & Huenemoerder, D. P. 1985, ApJ, 291, 72
Wilson, A. S., & Ulvestad, J. S. 1982, ApJ, 263, 576
Wilson, A. S., & Willis, A. G. 1980, ApJ, 240, 429
Wynn-Williams, C. G., Becklin, E. E., & Scoville, N. Z. 1985, ApJ, 297, 607